Dissertations and Theses   City College of New York

2021

Coordinated Control for DC Energy Hubs Involving DERs, EVs, and Subway Systems

Rohama Ahmad
CUNY City College

Coordinated Control for DC Energy Hubs Involving DERs, EVs, and Subway Systems

Thesis

Submitted in partial fulfillment of the requirements for the degree

Master of Engineering, Electrical

At

The City College of the City University of New York

By

Rohama Ahmad

June 2021

Prof. Ahmed Mohamed, Thesis Advisor

Prof. Roger Dorsinville, Chair Dept. of Electrical Engineering

Coordinated Control for DC Energy Hubs Involving DERs, EVs, and Subway Systems

Rohama Ahmad

Dept. of Electrical Engineering

Coauthors: Ahmed Ali A. Mohamed[1,2], Senior Member, IEEE, Hegazy Rezk[3], and Mujahed Al-Dhaifallah[4]

Thesis Advisor: Prof. Ahmed Mohamed

[1]City University of New York, City College, New York, NY 10031 USA

[2]Department of Electrical Engineering, Minia University, Minia, Minia 61512 Egypt

[3]Systems Engineering Department, King Fahd University of Petroleum & Minerals, Dhahran 31261 KSA

[4]College of Engineering at Wadi Addawaser, Prince Sattam Bin Abdulaziz University, Wadi Aldawaser 11991 KSA

Abstract

In this paper, a decentralized DC microgrid solution is proposed to mitigate high penetration levels of distributed energy resources (DERs) and Electric Vehicles (EVs). The microgrid is further expanded to integrate the regenerative energy available as a result of train braking at adjacent subway lines. Therefore, the proposed configuration helps the distribution network accommodate more renewable energy and reduces the energy consumption and peak demand associated with the electrified transportation. A framework for DC microgrid control has been developed and evaluated using a case study. The results prove the validity and effectiveness of the proposed control framework. In addition, the proposed energy hub has the potential to recuperate a substantial amount of the subway regenerative braking energy.

Table of Contents

Index Terms

Control, DERs, EVs, finite state machines, regenerative braking, subway

List of Figures

List of Tables

I. Introduction

Power systems worldwide are undergoing unprecedented advances to achieve two main goals. The first is to increase power system resilience, while the second is to confront global temperature increase. To accomplish the first goal, end users must have their own generators and energy storage systems (ESS) to provide energy to their loads during public electricity failure in the form of microgrids. Microgrids are interconnected through the main power network during normal operating conditions but can work independently during blackouts [1]. The second goal can be accomplished by increasing the renewable energy sources and electric vehicles. Nowadays, many countries worldwide aim at using alternatives to the fossil fuels such as new, renewable and environment-friendly energy sources. With these new resources and the deployment of microgrids, economic, environmental and societal benefits as well as improving the system's resilience can be achieved [2].

Several countries around the world have set up aggressive goals to increase the penetration levels of renewable energy, such as the Kingdom of Saudi Arabia's (KSA) Vision 2030. In order for the KSA to meet its 2030 renewable energy goals, a more substantial fraction of the total energy production will be contributed from renewable resources [3]. Moreover, with the rapidly evolving electric vehicle (EV) technologies and dropping battery cost, more EVs are expected on the KSA's roads within the coming few years. Both renewable energy and electric vehicles impose a set of looming challenges to power grid operators. Renewable energy sources are intermittent by nature adversely affecting the power grid, unless they are augmented with energy storage. In addition, EV charging is expected to strain the distribution network. The solution to these challenges requires development of a set of optimal control strategies and energy management algorithms to reliably operate the power grid taking into account renewable energy sources, moving as well as stationary electric vehicles, controllable loads, and other major loads (e.g., electrified transportation and/or heating) [4-6].

In this paper, a coordinated control framework for DC energy hubs, involving DERs, EVs, and subway power supply [7], has been proposed. The proposed framework has been validated using a case study. The rest of the paper is organized as follows: in section II, an overview of the challenges associated with electrified transportation has been provided; section III focuses on the DC energy hub concept; in section IV, the case study will be described; in section V, the results and discussion will be presented; finally, in section VI, the main conclusions of this study will be summarized.

II. Electrified Transportation

A. Electric Vehicles

EV chargers vary in their power ratings from the sub-kW to 20kW range for Levels 1 and 2 chargers, and up to 400kW for DC fast charging. EVs can collectively represent a significant demand increase when charging, ultimately mandating wide scale distribution infrastructure upgrade. Infrastructure upgrade can be deferred and the impact of EVs can be mitigated, if they are intelligently managed and their charging/discharging process is coordinated and optimally scheduled. Home charging is likely to take place during late evening through early morning, leading to a time shift in the residential load peak.

B. Subway

Subway power systems are large consumers of electricity. For instance, the average energy consumption in New York City is about 1.8 billion kWh per year with approximately 495,000 kW required by the subway system for operation during peak hours. The subway trains are powered via power lines in the form of third rails that run in parallel to traction rails or overhead catenaries. The power lines receive the DC power from a set of rectifier substations that are distributed throughout the subway line. In 650-V DC systems, the rectifier substations include transformers that steps down the medium voltage utility distribution voltage to about 490-V. Transformers are followed by uncontrolled rectifiers providing the DC voltage. With no train load, the voltage is typically close to 650-V but as the train approaches or departs from the station, the voltage on the third rail fluctuates.

Most modern rolling stock is equipped with regenerative braking capability. Unlike friction-based braking, regenerative braking enables a portion of the kinetic energy stored in the train inertia to be recaptured and potentially injected back to the third rail during train deceleration [8].

If a load happens to exist close enough to the decelerating train on the third rail (e.g., an accelerating train at the same passenger station), it will draw the injected energy. However, if there is no load, the third rail voltage tends to rise causing the protection system to electrically disconnect the train from the third rail. Analysis of large subway systems, such as the New York City system, concluded that regenerative braking energy results in only about 8%-9% energy saving [9]. The proposed DC energy hub will help recuperate more regenerative braking energy due to the connected load, wayside ESS, and reversible path to the main AC grid through the inverter.

III. DC Energy Hub

A. Motivation

DERs are typically integrated on the distribution level, which already on its current status represents a weak ring the power delivery chain, i.e. some of its deficiencies include lack of automated analysis, poor visibility, lack of situational awareness, and slow response time. Experiences also show that the hierarchically central control of the power systems significantly contributed to the blackouts that took place in last century. Since grid-scale energy storage systems (ESS) are still not cost-efficient, the electric power has to be generated and consumed in real-time. This has been doable through accurate load forecasting models, and relatively fast generation control and frequency stabilizers. However, with high penetration of DERs and EVs, given their uncertainty, the grid operator will have difficulty maintaining the load/generation balance and consequently the stability of the system, which may compromise the whole network reliability.

In order to overcome this problem, the grid would hypothetically have to communicate with all the DERs in real-time and coordinate their operation, which is not practical since the massive amount of date that will need to be transmitted will represent a bottle-nick for any communication technology. A feasible solution is to offload the control and communication from the utility, and optimize the DERs locally within local energy networks, typically referred to as microgrids [10] (see Figure 1).

Microgrid assets can be integrated using a common AC bus or a common DC bus. DC bus integration provides several advantages, including enhanced overall efficiency of the system due to the reduced number of conversion stages; enhanced power-carrying capacity of cables due to lack of reactive power related voltage drop; reduced cable resistance due to lack of skin effect; and eliminating the need for var control [11].

B. Topology

The proposed DC energy hub consists of a solar system interfaced with the common DC bus through a DC-DC converter controlled to perform Maximum Power Point Tracking (MPPT); a battery interfaced with a bi-directional DC-DC converter controlled via a battery management system (BMS), EV chargers, connection to the third rail, AC and DC loads, and bi-directional four-quadrant connection to the main grid.

C. Third Rail Integration

Consider the typical interval metering data profile depicted in Figure 2, for a real subway substation in New York City. It can be observed that there is enough energy during off-peak hours to charge EVs and electric buses (e.g., the shaded area only is about 4MWh), without altering the peak power. Notice that this behavior repeats (see Figure 3). EVs can charge behind the same traction meter (with the same demand charges being encountered by trains), instead of

being charged separate demand charges behind another meter at the bus depot. Therefore, the proposed DC energy hub increases the recuperation of regenerative braking energy while mitigating the impact of EV charging on the electricity distribution grid.
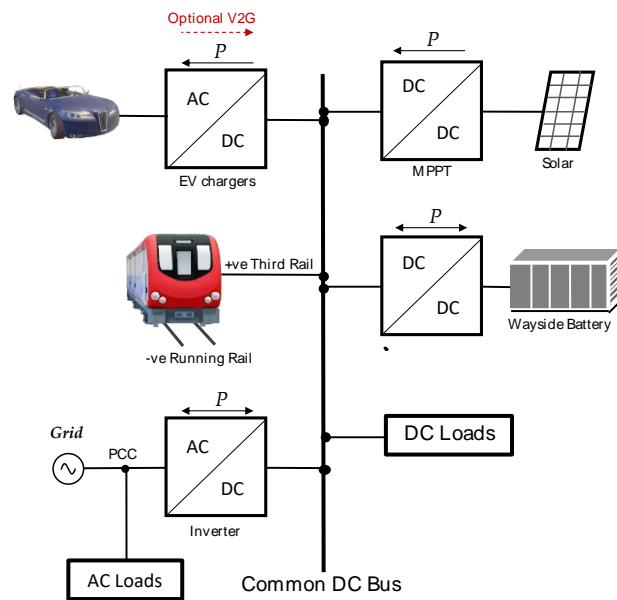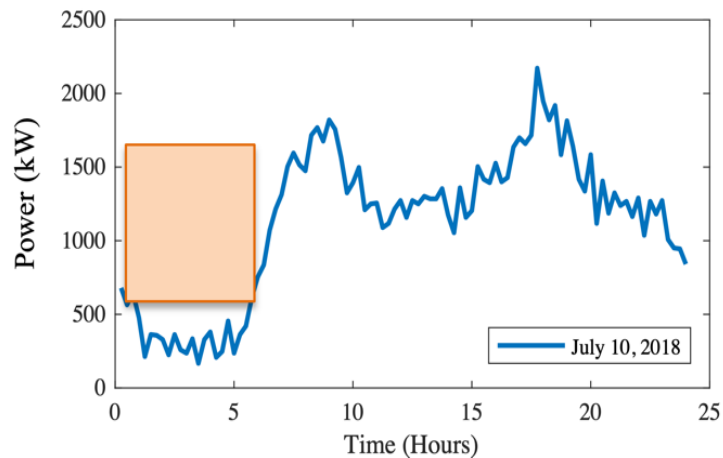

Figure 1: Common DC bus integration

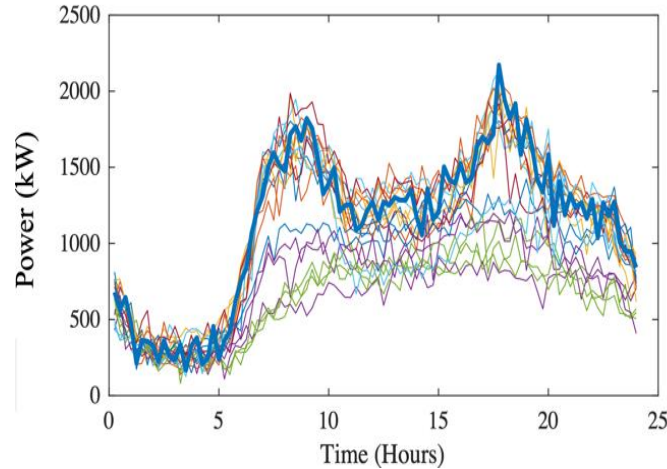Figure 2: Interval metering data for a sample summer day of a substation

Figure 3: Interval metering data for 20 sample days of a subway substation

IV. Control Framework

The case study follows the layout depicted in Figure 4. The parameters of the converters and controllers are summarized in Table I. The control hierarchy consists of two levels, a set of local controllers and a single secondary orchestrator, with the possibility for the secondary orchestrator to coordinate with an external tertiary controller (e.g., the utility grid or a community aggregator).

In this hierarchy, the local controllers carry out local tasks, by regulating the voltage, current, and/or power corresponding to pre-specified setpoints and local sensor measurements, while the secondary orchestrator optimizes the overall system performance by finding those optimal setpoints and sending them to the local controllers. Hence, the bandwidth requirements for the controllers and the vulnerabilities to single point failure are substantially reduced.

The photovoltaic (PV) system modeled in this case study consists of A10 Green Technology (A10J-S72-175) modules, forming 40 parallel strings, 10 series-connected modules per String, and 72 cells per module. The maximum power is 175 W. The boost converter interfacing the PV system performs maximum power point tracking (MPPT), using the Perturb and Observe

algorithm. The initial duty cycle is 0.87, the initial voltage is 80 V, and the initial power is 640

W. To model EV charging load, a buck-boost converter, controlled using a proportional-integral

(PI) controller, is used to draw power based on a regulated DC load voltage (480 V in Fig. 4).

One of key components in this system is the inverter, tying up the common DC bus with the

AC grid. Since the inverter will be required to operate in four quadrants, it needs to utilize a

vector-decoupling pulse-width-modulation (PWM) technique. Vector-decoupling control

requires coordinate transformation to the d-q frame of references. The voltage equation of a

three-phase PWM converter is as follows,

$$e_s = Ri_s + L\frac{di_s}{dt} + v_r \tag{1}$$

where

e_s = source voltage

i_s = source current

v_r = converter input voltage

R, L = resistance and inductance of the boosting inductor, respectively.

$$L\frac{di_{de}}{dt} - wLi_{qe} + Ri_{de} = e_{de} - v_{de} \tag{2}$$

$$L\frac{di_{qe}}{dt} - wLi_{de} + Ri_{qe} = e_{qe} - v_{qe} \tag{3}$$

where w = voltage source angular frequency

For fast voltage control, the input power should supply instantaneously the sum of load power

and charging rate of the capacitor energy. Neglecting the resistance loss and the switching device

loss, the power balance between the ac input and the DC output is as follows

$$P = \frac{3}{2}(e_{de}i_{de} + e_{qe}i_{qe}) = v_{dc}i_{dc} \qquad (4)$$

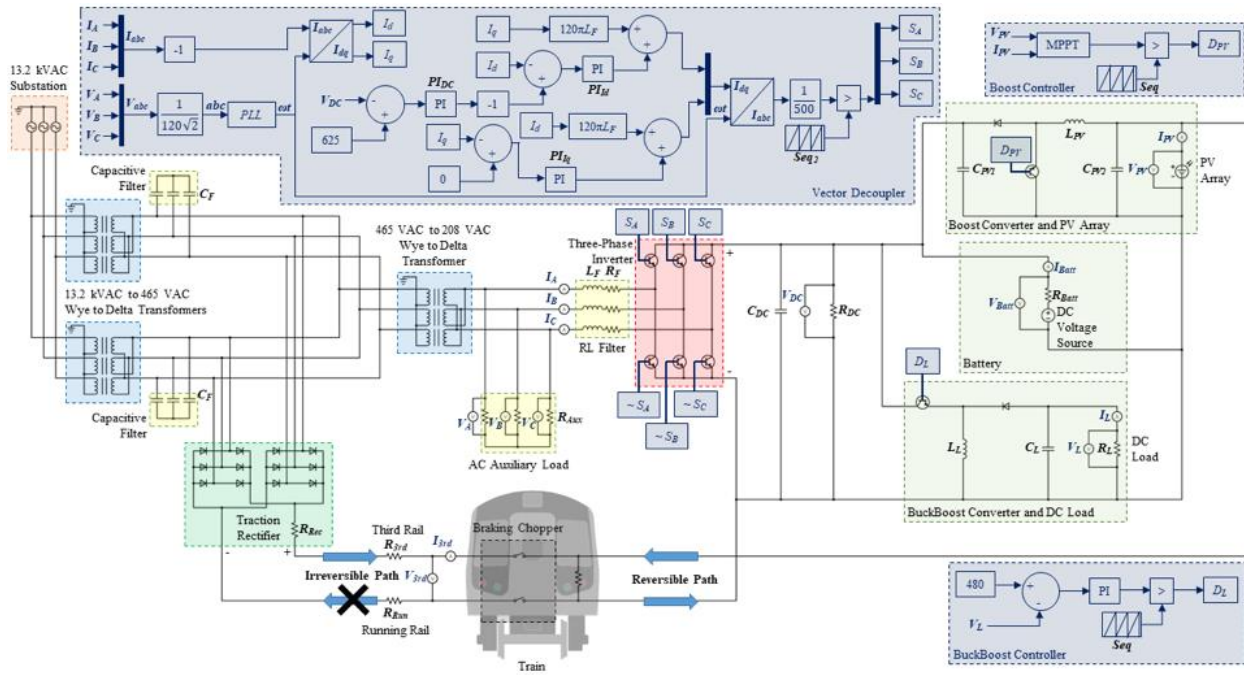where v_{dc}, i_{dc} = DC output voltage and current, respectively.

Figure 4: Schematic diagram of the system under study

TABLE I
PARAMETERS OF THE SYSTEM UNDER STUDY

Symbol	Quantity	Value
C_F	Capacitive Filter's Capacitance	1 mF
R_{Rec}	Traction Rectifier's Internal Resistance	1.08mΩ
R_{3rd}	Third Rail's Resistance	25mΩ
R_{Run}	Running Rail's Resistance	12mΩ
R_{Aux}	AC Auxiliary Load's Resistance	40Ω
L_F	RL Filter's Inductance	3mH
R_F	RL Filter's Resistance	1Ω
C_{DC}	DC Bus Capacitor's Capacitance	12mF
R_{DC}	DC Bus Resistor's Resistance	60Ω
C_{PV1}	Boost Converter Capacitor 1's Capacitance	0.27mF
C_{PV2}	Boost Converter Capacitor 2's Capacitance	0.27mF
L_{PV}	Boost Converter Inductor's Inductance	8.5mH
R_{Batt}	Battery's Internal Resistance	5mΩ
L_L	Buckboost Converter Inductor's Inductance	0.8mH
C_L	Buckboost Converter Capacitor's Capacitance	1.2mF
R_L	DC Load's Resistance	20Ω
R_L	DC Load's Resistance	20Ω
K_p	Buckboost PI Controller's Proportional Gain	0.001
K_i	Buckboost PI Controller's Integral Gain Value	0.1
Kp_{PIdc}	PI_{DC} Controller's Proportional Gain	0.1
Ki_{PIdc}	PI_{DC} Controller's Integral Gain	1
Kp_{PIIq}	PI_{Iq} Controller's Proportional Gain	30
Ki_{PIIq}	PI_{Iq} Controller's Integral Gain	240
Kp_{PIId}	PI_{Id} Controller's Proportional Gain	30
Ki_{PIId}	PI_{Id} Controller's Integral Gain	240
Seq	Repeating Sequence 1 (Frequency)	10 kHz
Seq	Repeating Sequence 1 (Range)	[0 1]
Seq_2	Repeating Sequence 2 (Frequency)	10 kHz
Seq_2	Repeating Sequence 2 (Range)	[-1 1]

On the dc output side,

$$i_{dc} = -C\frac{dv_{dc}}{dt} - i_L \qquad (5)$$

where i_L is the load current. From (4) and (5),

$$\frac{3}{2}(e_{de}i_{de} + e_{qe}i_{qe}) = -Cv_{dc}\frac{dv_{dc}}{dt} - v_{dc}i_L \qquad (6)$$

In order to enhance the performance of the current control loops, the decoupling term (wLi_{de}) and (wLi_{qe}) were included while calculating $v_{rq}{}^{cont}$ and $v_{rd}{}^{cont}$, respectively. These voltages are the modulation signals for the PWM technique. The equations used in building the controller are given by (7), as shown in Fig. 4.

$$v_{rq}{}^{cont} = wLi_{de} + e_{qe} - Ri_{qe} - K_p \cdot [i_{de}{}^{ref} - i_{de}] - K_i \cdot \int [i_{de}{}^{ref} - i_{de}]dt \qquad (7)$$
$$v_{rd}{}^{cont} = -wLi_{qe} - Ri_{qe} - K_p \cdot [i_{de}{}^{ref} - i_{de}] - K_i \cdot \int [i_{de}{}^{ref} - i_{de}]dt$$

To synchronize the inverter output with the grid and enable vector decoupling, a phase locked loop (PLL) is used to detect the grid phase angle using the measured voltage. The phase angle is used to decouple current and voltage signals, and to convert them back to the a-b-c frame of references at the end of the control loop. A nested control loop is used, in which a voltage controller attempts to regulate the common DC bus voltage. The output of the voltage PI controller serves as a reference for an internal direct-axis current controller. The quadrature-axis current is set to zero in Fig. 4, to operate at unity power factor, but can be set up to provide capacitive or inductive reactive power support if needed.

The train power supply system consists of an uncontrolled rectifier substation, connecting the power utility medium voltage (13.2 kV AC in this case) to two three-phase transformers stepping down the voltage to about 500V, followed by two full-bridge diode-based rectifiers for redundancy. A capacitive filter is connected between the transformers and the rectifiers. The output of the uncontrolled rectifiers forms the third-rail voltage. The positive of the rectifiers is connected to the third rail, while the running rails represent the return path. The train has

onboard choppers to enable dynamic braking if regenerative braking is not possible. The output

of the transformers is also connected to the AC point of the inverter linking the common DC bus.

As for the secondary orchestrator, we have expanded our finite-state-machine (FSM) based

microgrid controller presented in [12], [13], to accommodate regenerative braking energy. The

proposed controller in [12] and [13] optimizes the system performance through forecasting and

ESS/load scheduling, so that the overall cost of energy and the resiliency are both optimized. It

performs energy arbitrage, peak demand scheduling, etc. The focus of this paper is on the

relatively new aspect of integrating the train system. A FSM contains permissible inputs, initial

state, final state and output (could also be null). For a deterministic FSM, the final state and

output is a function of initial state and input. FSM of a railway system is deterministic since the

final state and output are the result of the initial state and the action of permissible inputs. A

mathematical expression for FSM is a five-tuple: $(X, Y, S, \delta, \lambda)$, X is the input set, Y is the

output set, S is the states set, δ is the transition set and λ is the output function. FSM can also be

expressed as a State Transition Table (STT). The STT contains input, initial state, final state and

output. We combine the five-tuple and STT representations in this work.

The following format is used to describe the FSM: $M = (S, T, s_0)$. S is a finite set of states. T is

a set of transitions. $T: s_{initial} \rightarrow s_{final}$. s_0 is a set of initial states. $s_{initial}, s_{final}, s_0 \in S$

For simplicity, the system can be divided into multiple layers. For instance, for a hybrid ESS two

layers can be used, with three-major states (upper) and subsystems (lower). The three-major

states contain neutral, charge and discharge states. Subsystems contain the charging subsystem

and the discharging subsystem.

$$M1 = (\{s_0, s_1, s_2\}, \{a, b, c, d\}, s_0)$$

$$M2 = (\{s_1, s_3, s_4, s_5\}, \{e, f, g\}, s_1)$$

$$M3 = (\{s_2, s_6, s_7, s_8\}, \{h, i, j\}, s_2)$$

M1 is for the three-major states. M2 is for subsystem of charge. M3 is for the subsystem of

discharge.

When a train approaches the station, it decelerates injecting current to the third rail. The

controller should detect the rise in the voltage and charge the ESS before the voltage reaches to

its upper limit. On the other hand, when a train is departing the station, it draws current and the

voltage tends to fail. The controller should attempt to discharge the battery. Figure 5 shows state

transitions for the three-major states. The major states and their STT are presented in Tables II

and III. Further details of the states and transitions are provided in the Appendix.
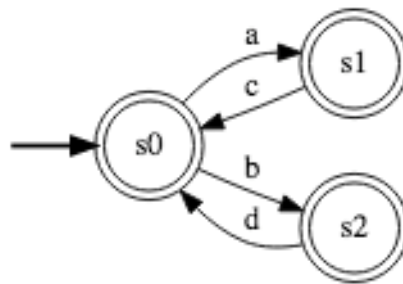

Figure 5: Major states

TABLE II
SET OF MAJOR STATES

Symbol	State
S0	Neutral
S1	Charge
S2	Discharge

TABLE II
STATE TRANSITIONS FOR THE MAJOR STATES

Transition	Inputs			
	V	SOC	Itrain	
a	V>Vc	SOC<95%	Itrain<0	charge
b	V<Vdisc	SOC>20%	Itrain>0	discharge
c	V<=590		Itrain>0	
c		SOC>=95%		neutral
d	V>690		Itrain<0	
d		SOC<=20%		

V. Results and Discussion

In order to examine the performance of the proposed DC energy hub solution, transient simulations were performed using MATLAB/SIMULINK. The system was tested under varying operating conditions of solar radiation, EV charging, and a train acceleration/deceleration cycle. The DC load voltage is depicted in Fig. 6. As can be seen, the buck-boost converter is capable of regulating the voltage through the simulation time. This results in a constant EV charging power of about 12 kW, as shown in Fig. 7. This implies that the load is unaffected by the variations in power/voltage on the common DC bus, which are caused by the PV variation and train motion. The PV irradiance and temperature conditions were varied, as shown in Figs. 8 and 9, respectively.

One of the main functions of the battery in this system is to act as a wayside ESS for the train. The train departs the station, typically accelerating at a rate of around 2.5 MPH/s. This results in

a large draw of current/power that normally leads to a dip in the DC bus voltage. The battery needs to discharge current during this time. Also, a train approaching the station decelerates, typically at a rate of around -3 MPH/s. This results in a large impulse of current injected to the third rail in about 30 seconds. If not timely captured, the voltage rises and the protection system disconnects the train electrically. The battery will help regulate the DC bus voltage such that it provides current when the train is accelerating. Ideally, the battery current resembles the train demand, as shown in Fig. 10.

Figure 11 depicts the performance of the PLL. It can be seen that the PLL is able to accurately detect the grid phase angle. This is fed to the controller to solve Park's equations. Figure 12 shows the voltage of the common DC bus. It can be seen that the voltage is maintained within about 595V-640V. This range is acceptable both for the operation of the PV, ESS, and EV, and also to enable maximum recuperation of train regenerative braking energy. The voltage has a large dip that starts at about 30s when the train starts to accelerate. The voltage dip is detected and the battery discharges power to help regulate the DC bus voltage. The dip ends when the train reaches its maximum speed. At about 58s, the voltage starts to rise when the train is decelerating approaching the station. The battery charges during this time to capture regenerative braking energy and regulate the voltage.

Figure 13 provides a more detailed description of the power response for the various assets. It can be seen that the battery changes from discharge to charge corresponding to the train movement, with minimal intervention from the substation (denoted third-rail current), and that the load and PV power are unaffected throughout these train power variations. Figure 14 provides a zoomed-in view for Fig. 13.
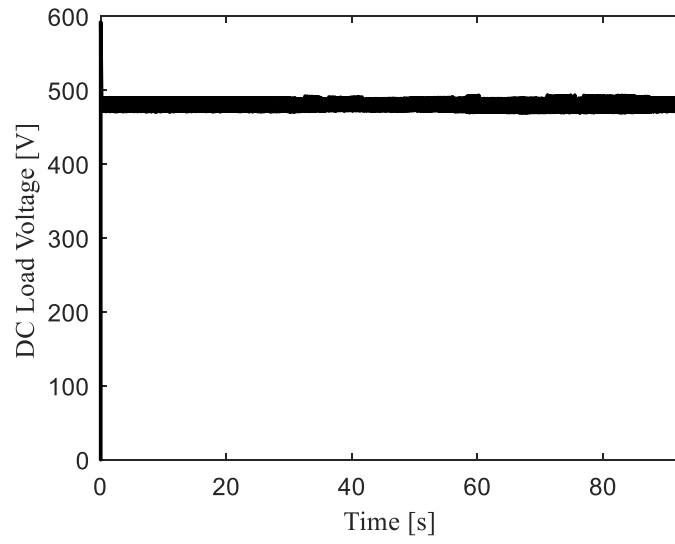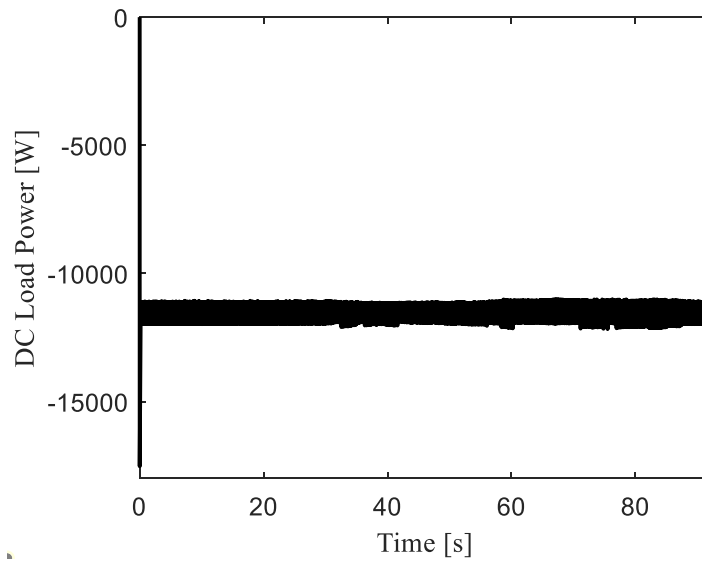
Figure 6: The DC load voltage
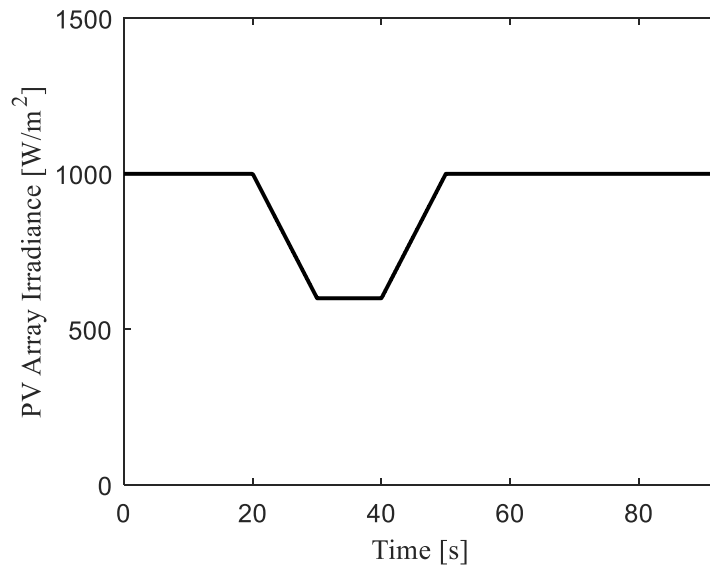

Figure 7: The DC load power

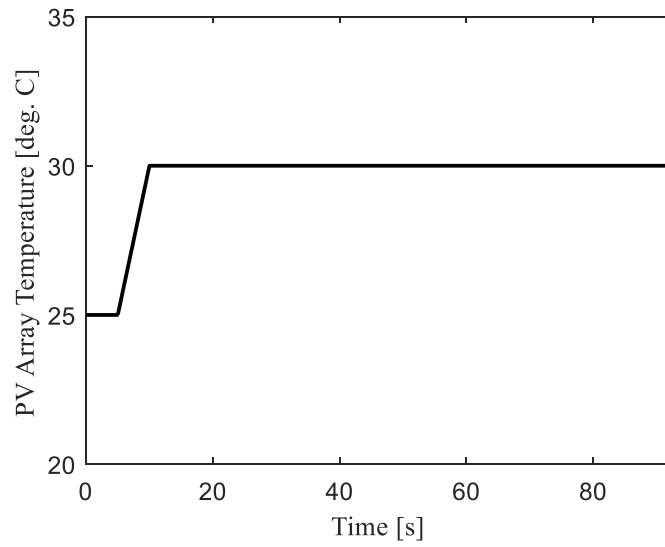Figure 8: PV irradiance variation over time

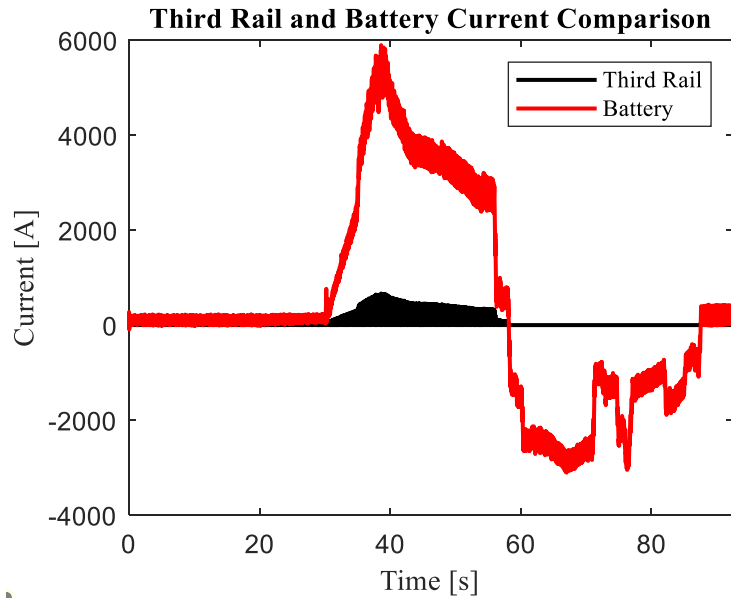Figure 9: PV temperature variation over time
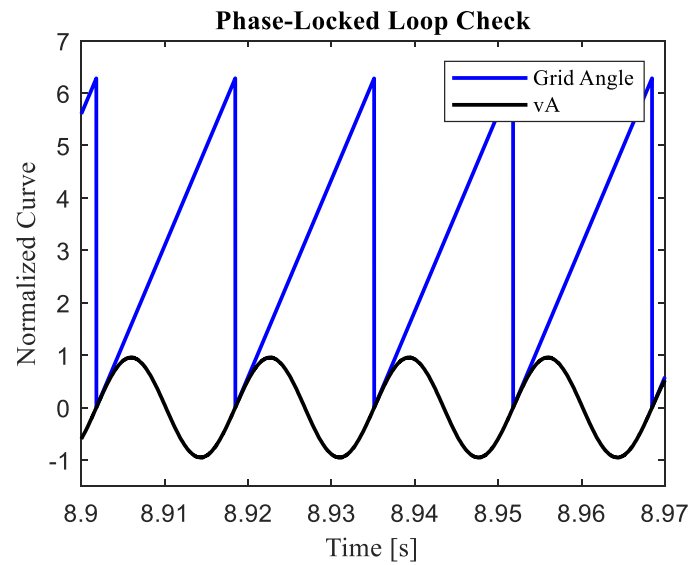
Figure 10: Third rail and ESS currents

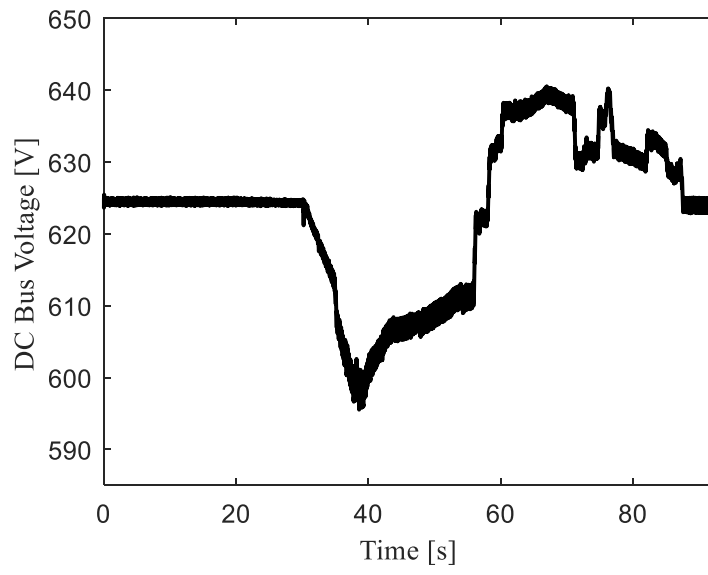Figure 11: PLL operation to detect the grid phase angle
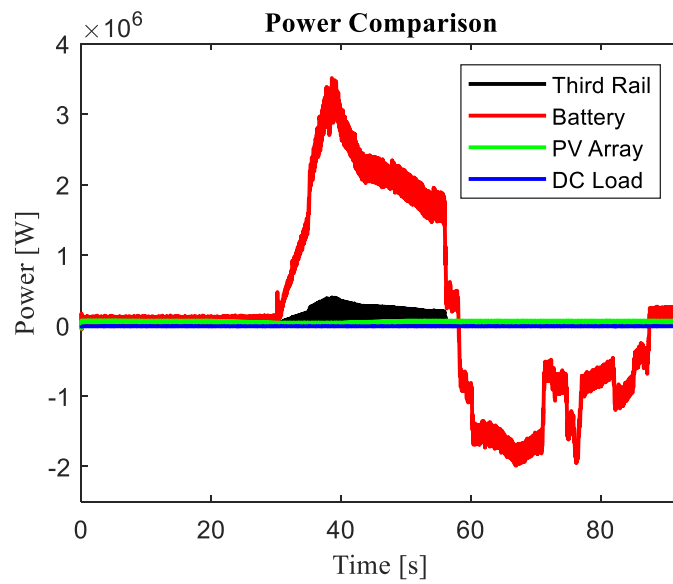
Figure 12: Common DC bus voltage

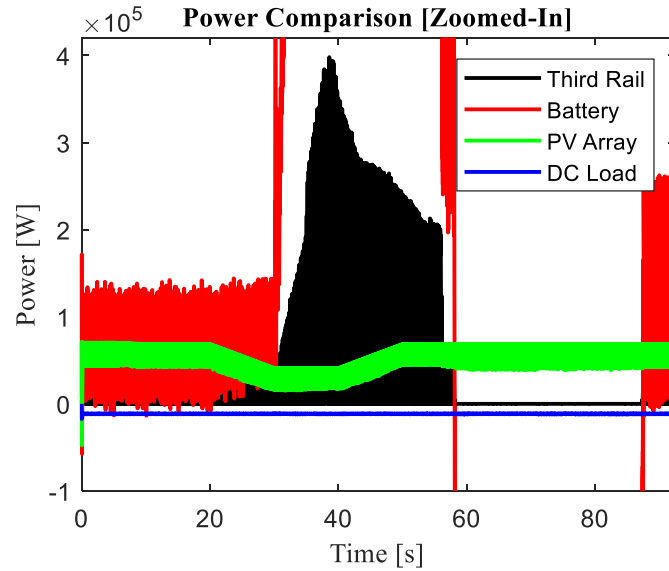Figure 13: Output power of the DC energy hub assets

Figure 14: A Y-Axis zoomed-in view for the output power of the DC energy hub assets

VI. Conclusion

In this paper, a DC energy hub solution was proposed to integrate photovoltaic, energy storage, electric vehicle charging load, and train power supply into a common DC bus. The system was modeled and simulated. A case study was used to verify the applicability and effectiveness of the proposed solution. It was found that the system successfully mitigated the impact of photovoltaic intermittency, managed the EV load, and maintain a regulated common DC bus voltage. In addition, one of the key advantages of the proposed solution is that it enabled the regenerative braking energy available during train braking to flow to the DC bus, and further to the EV load, energy storage, or back to the grid through the reversible path formed by the inverter. This has the potential to substantially increase recuperation of regenerative braking energy improving the overall efficiency of the subway system.

Appendix

Figure A1 shows state transitions for the subsystem associated with charging. Figure A2 shows the state transitions for the subsystem associated with discharging. Tables AI and AII show definition of the states. V_c is the threshold to trigger charging and V_{disc} is that to trigger discharging. Table AIII shows transitions for the charging subsystem. Table AIV shows transitions for the discharging subsystem. Tables AV and AVI are the transition tables for the system.
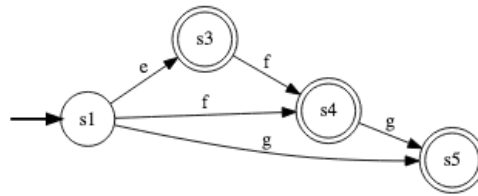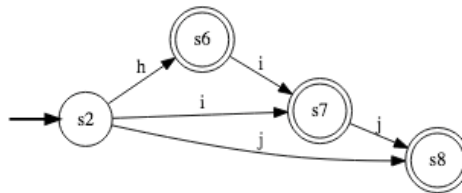

Figure A1: Subsystem for charging

Figure A2: Subsystem for discharging

TABLE AI
CHARGING SUBSYSTEM STATES

Symbol	State	
S1	initial state of Charge	
S3	Fast Speed Charge	
S4	Medium Speed Charge	charge
S5	Slow Speed Charge	

TABLE AII
DISCHARGING SUBSYSTEM STATES

Symbol	State	
S2	initial state of Discharge	
S6	Fast Speed Discharge	
S7	Medium Speed Discharge	discharge
S8	Slow Speed Discharge	

TABLE AIII
TRANSITIONS FOR CHARGING SUBSYSTEM STATES

Transition	Inputs			
	V	SOC	Itrain	
e	V>Vc	20%<SOC<60%	Itrain<0	
f	V>Vc	60%<SOC<90%	Itrain<0	charge
g	V>Vc	90%<SOC<95%	Itrain<0	

TABLE AIV
TRANSITIONS FOR DISCHARGING SUBSYSTEM STATES

Transition	Inputs			
	V	SOC	Itrain	
h	V<Vdisc	60%<SOC<95%	Itrain>0	
i	V<Vdisc	25%<SOC<60%	Itrain>0	discharge
j	V<Vdisc	20%<SOC<25%	Itrain>0	

TABLE AV
STT FOR CHARGING SUBSYSTEM STATES

Transition	e	f	g
S1	S3	S4	S5

TABLE AV
STT FOR DISCHARGING SUBSYSTEM STATES

Transition	h	i	j
S2	S6	S7	S8

References

[1] K. Thirugnanam, M. S. E. Moursi, V. Khadkikar, H. H. Zeineldin and M. Al Hosani, "Energy Management of Grid Interconnected Multi-Microgrids Based on P2P Energy Exchange: A Data Driven Approach," in *IEEE Transactions on Power Systems*, vol. 36, no. 2, pp. 1546-1562, March 2021, doi: 10.1109/TPWRS.2020.3025113.

[2] O. Dutta and A. Mohamed, "Reducing the Risk of Cascading Failure in Active Distribution Networks Using Adaptive Critic Design," IET Generation, Transmission & Distribution, vol. 14, no. 13, pp. 2592-2601, July 2020.

[3] Available Online at: https://www.vision2030.gov.sa/ (Last Accessed: May 2021).

[4] P. J. d. S. Neto, T. A. d. S. Barros, J. P. C. Silveira, E. R. Filho, J. C. Vasquez and J. M. Guerrero, "Power Management Strategy Based on Virtual Inertia for DC Microgrids," in *IEEE Transactions on Power Electronics*, vol. 35, no. 11, pp. 12472-12485, Nov. 2020, doi: 10.1109/TPEL.2020.2986283.

[5] M. Nasr, E. Nasr-Azadani, H. Nafisi, S. H. Hosseinian and P. Siano, "Assessing the Effectiveness of Weighted Information Gap Decision Theory Integrated With Energy

Management Systems for Isolated Microgrids," in *IEEE Transactions on Industrial Informatics*, vol. 16, no. 8, pp. 5286-5299, Aug. 2020, doi: 10.1109/TII.2019.2954706.

[6] M. Jafari, Z. Malekjamshidi, J. Zhu and M. Khooban, "A Novel Predictive Fuzzy Logic-Based Energy Management System for Grid-Connected and Off-Grid Operation of Residential Smart Microgrids," in *IEEE Journal of Emerging and Selected Topics in Power Electronics*, vol. 8, no. 2, pp. 1391-1404, June 2020, doi: 10.1109/JESTPE.2018.2882509.

[7] M. Khodaparastan, O. Dutta, M. Saleh and A. Mohamed, "Modeling of DC Electric Rail Transit Systems with Wayside Energy Storage," IEEE Transactions on Vehicular Technology, vol.68, no. 3, pp. 2218-2228, March 2019.

[8] M. Khodaparastan, W. Brandauer and A. Mohamed, "Recuperation of Regenerative Braking Energy in Electric Rail Transit Systems," IEEE Transactions on Intelligent Transportation Systems, vol. 20, no. 8, pp. 2831-2847, Jan. 2019.

[9] A. Mohamed, A. Reid, and T. Lamb, "White Paper on Wayside Energy Storage for Regenerative Braking Energy Recuperation in the Electric Rail System," published by Consolidated Edison, Inc., August 2018, Available online at: https://www.coned.com/-/media/files/coned/documents/our-energy-future/our-energy-projects/regenerative-braking-energy-recuperation.pdf. (Last Accessed: May 2021)

[10] N. Wu, H. Wang, L. Yin, X. Yuan and X. Leng, "Application Conditions of Bounded Rationality and a Microgrid Energy Management Control Strategy Combining Real-Time Power Price and Demand-Side Response," in *IEEE Access*, vol. 8, pp. 227327-227339, 2020, doi: 10.1109/ACCESS.2020.3045754.

[11] S. Zeinal-Kheiri, A. M. Shotorbani and B. Mohammadi-Ivatloo, "Real-time Energy Management of Grid-connected Microgrid with Flexible and Delay-tolerant Loads,"

in *Journal of Modern Power Systems and Clean Energy*, vol. 8, no. 6, pp. 1196-1207, November 2020, doi: 10.35833/MPCE.2018.000615.

[12] M. Saleh, Y. Esa and A. Mohamed, "Impact of Communication Latency on the Bus Voltage of Centrally Controlled DC Microgrid during Islanding," IEEE Transactions on Sustainable Energy, vol. 10, no. 4, pp. 1844-1856, Oct. 2019.

[13] M. Saleh, Y. Esa and A. Mohamed, "Impact of Communication Latency on the Bus Voltage of Centrally Controlled DC Microgrid during Islanding," IEEE Transactions on Sustainable Energy, vol. 10, no. 4, pp. 1844-1856, Oct. 2019.